VTT Technical Research Centre of Finland

Mechanical behavior of high-Ni/high-Mn Barsebäck 2 reactor pressure vessel welds after 28 years of operation

Lindqvist, Sebastian; Norrgård, Alex; Arffman, Pentti; Hytönen, Noora; Lydman, Jari; Efsing, Pål; Suman, Siddharth; Nevasmaa, Pekka

Published in:
Journal of Nuclear Materials

DOI:
10.1016/j.jnucmat.2023.154447

Published: 01/08/2023

Document Version
Publisher's final version

Journal of Nuclear Materials 581 (2023) 154447

Contents lists available at ScienceDirect

Journal of Nuclear Materials

journal homepage: www.elsevier.com/locate/jnucmat

Mechanical behavior of high-Ni/high-Mn Barsebäck 2 reactor pressure vessel welds after 28 years of operation

Sebastian Lindqvist *, Alex Norrgård, Pentti Arffman, Noora Hytönen, Jari Lydman, Pål Efsing, Siddharth Suman, Pekka Nevasmaa

VTT Technical Research Centre of Finland Ltd, 02150 Espoo, Uusimaa, Finland

ARTICLE INFO

Keywords:
Surveillance
Mechanical properties
High-Ni/Mn weld
Embrittlement
Transition temperature
Impact toughness
Strength

ABSTRACT

To assess long-term operation of the reactor pressure vessel (RPV), surveillance programs are applied for periodic monitoring and prediction of the aging of the mechanical properties due to irradiation and thermal embrittlement. In literature, there are limited data sets to compare the results from the surveillance program to the aging of the RPV. In this work, the tensile and impact toughness properties of the high-Ni, high-Mn welds from decommissioned Barsebäck 2 RPV are characterized. The results indicate that the surveillance program describes sufficiently the aging of the RPV welds. Differences in mechanical properties of the welds from various regions are explained by variations in post-weld heat treatment. The synergetic effect of Ni and Mn on embrittlement appears not to result at low fluences in a significant difference in the embrittlement rate when compared to ASTM E900 embrittlement trend curve prediction.

1. Introduction

The reactor pressure vessel (RPV) is a life-limiting component in nuclear power plants (NPP). The RPV operates in an environment making it susceptible to irradiation and thermal embrittlement. As a consequence, hardness and strength increase, and the fracture toughness decreases. The effect of embrittlement on fracture properties and strength of the reactor pressure vessel (RPV) are monitored in surveillance programs where samples are placed in the RPV. The samples are extracted and tested at constant intervals to ensure that the material properties sustain a sufficient margin for stable operation. In the irradiation positions, the materials are typically subjected to a higher fluence compared to the RPV wall. The aim is to form a predictive embrittlement trend curve to assess long-term operability [1–3].

The surveillance program includes the limiting RPV materials [4]. The surveillance base metals are extracted from the actual forgings or plates by cutting a section before the RPV is assembled. The surveillance weld samples are extracted from a separate weld manufactured using the same welding parameters and materials. The base metal specimens tend to be extracted at ¼ thickness location to minimize material variability, but for welds, due to less variance in properties in the through-thickness direction, the samples are extracted from different depth locations. Noticeably, the properties of the weld root and the region close to the cladding tend to differ from the bulk properties and are thus excluded [4]. Though, from a structural integrity point of view, these regions are favorable as toughness can be higher and realistic flaws can be located in these regions.

The results from the surveillance program are compared to the embrittlement trend curves (ETC) that are derived from large experimental data bases, and the ETCs are usually analytical solutions dependent on chemistry and fluence. These analytical ETC perform relatively well as long as the chemical content of the material and fluence is in the spectrum of the applied method [3]. However, high-Ni/Mn welds common in many Nordic NPPs (Ni ≈1.5 % and Mn >0.8 %) and in the VVER-1000 designs can be outside the applicability limit of internationally recognized ETCs. The synergetic effect of Ni and Mn on embrittlement tends not to be accounted for, which can lead to biased prediction of the embrittlement behavior [5]. For this reason, data driven ETC are also accepted, where the results from the surveillance program have provided a firm enough basis for a case specific trend curve. The cost to obtain such a curve is higher.

The increased Ni content gives better hardenability and lower DBT temperature, but increases the sensitivity of the material to radiation embrittlement [6]. The increase in embrittlement rate is linked to the

* Corresponding author.
E-mail address: sebastian.lindqvist@vtt.fi (S. Lindqvist).

https://doi.org/10.1016/j.jnucmat.2023.154447
Received 1 March 2023; Received in revised form 10 April 2023; Accepted 12 April 2023
Available online 13 April 2023

synergetic effect of Ni and Mn, and also sometimes to Si [7]. In [5], they observe that the synergetic effect of Ni and Mn is activated after the combined content exceeds 2.9 %. The synergetic effect can also become more significant after Mn content exceeds 0.8 % [7], and Ni content exceeds 1.3 %, indicating that already at a combined content of 2.1 % the synergetic effect can be activated [8]. A relatively high temperature can also have a significant effect on the embrittlement rate for high Ni/Mn welds [9]. To further develop analytical ETCs for high-Ni/Mn welds, additional data is required. The significance of the synergetic effect is also related to the relative content of impurity elements such as Cu and P.

Studies on the through-thickness properties of beltline welds have been conducted for decommissioned Novovoronezh unit 1, Midland unit 1, and Greifswald units 1, 4 and 8 [10–15]. The results confirm that embrittlement curves based on chemical composition provide sufficient safety margins. However, in these programs, the results from the surveillance program are not compared to the mechanical behavior of the RPV, as these reactors never included an individual surveillance program. Compared to the surveillance capsules, the RPV wall is stressed due to the internal pressure and the RPV is subjected to a lower irradiation flux which can alter the aging response.

In this study, high-Ni/Mn welds from the decommissioned Barsebäck 2 RPV are investigated. The material is extracted from the RPV head, and the circumferential and axial beltline welds, enabling comparison between the RPV head (RPVH) material subjected to a high temperature (280°C) and the beltline region subjected to irradiation and a similar temperature. To minimize variability, the mechanical properties are characterized at ¼ thickness using instrumented Charpy-V testing done according to ISO 148-1 [16] and tensile testing done according to ISO 6892-1 [10]. The results are compared to the results from the surveillance program essential for long-term operation.

2. Methods and materials

This section introduces the characteristics of the investigated weld and the cutting plan for the impact toughness and tensile specimens. Also, the testing program is described in detail.

2.1. Materials

The Barsebäck 2 reactor was operated for 210 600 h at its peak operational pressure and temperature, equivalent to 22.7 efpy (effective full power years). The reactor vessel head temperature was close to 288°C and in the core region closer to 270°C. The head and beltline regions of the RPV are subjected to different degradation mechanisms, the head region is primarily subjected to thermal aging whereas the beltline region is subject to thermal aging and to neutron irradiation.

The Barsebäck 2 welds are double U-groove welds with the root removed. The investigated welds are primarily submerged arc welded (SAW) and manufactured using the same welding procedure. The RPVH welds were finished on the outer surface with manual metal arc (MMA) welding. The SAW region was welded using Phoenix-Union S3NiMo and MMA region with Oerlicon Tenacito 65. The investigations in this work focus on the SAW regions. Both materials are characterized by high-Mn/high-Ni content. Post weld heat-treatment (PWHT) was performed at 620 ± 15°C for approximately 5.5 h. Welding temperature was 175 ± 50°C. A short heat treatment was done after the welding 575 ± 25°C for minimum of 15 min and thereafter soaked at 250°C for minimum 16 h, before the PWHT.

For the experimental characterization program, weld trepans were cut from the Barsebäck RPV head (RPVH) and from the axial and circumferential beltline welds, see Fig. 1. The diameter of the trepan is 200 mm. The cladding was removed afterwards. The trepans were cut into slices at the ¼ thickness location from where the test specimens were cut, see Fig. 2. The fluence after operation for the extracted axial beltline weld trepan is $7.9{\cdot}10^{17}$ n/cm^2 (E > 1 MeV) at the surface and

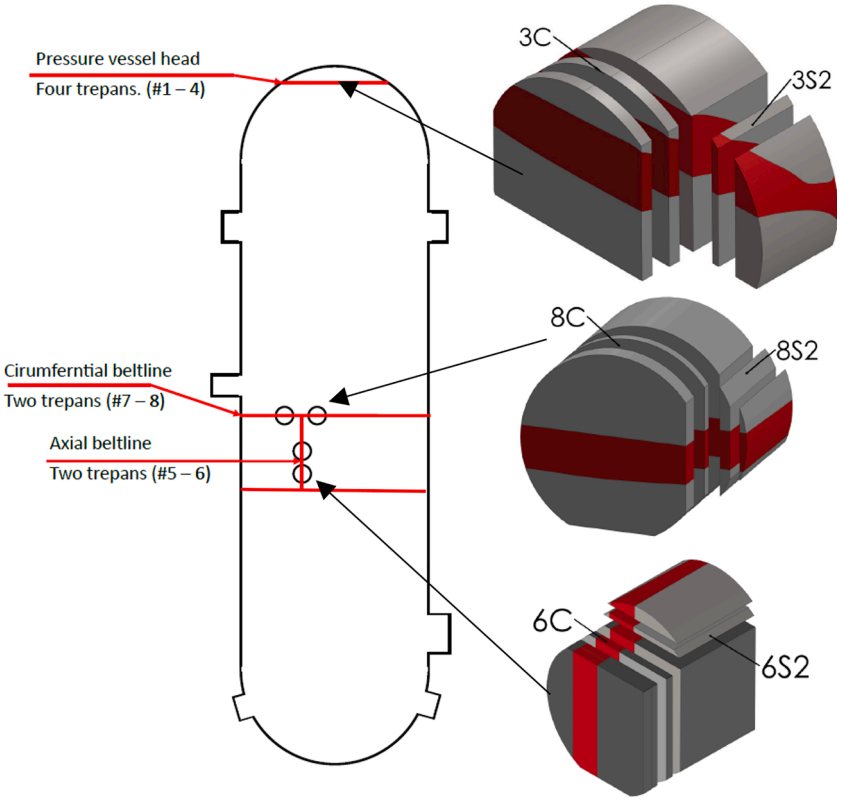

Fig. 1. Trepan extraction locations from Barsebäck 2 RPV. Red regions illustrate the weld seam in the trepan.

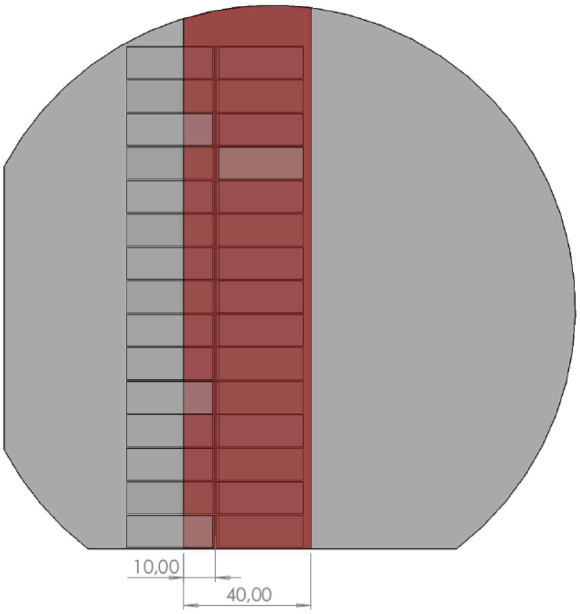

Fig. 2. Demonstrates the location of the impact toughness specimens cut form the sliced trepan.

$2.9{\cdot}10^{16}$ n/cm^2 (E > 1 MeV) for the circumferential beltline weld trepan. The RPV thickness is 126 mm in the beltline region and 70 mm in the RPVH. The thickness of the cladding is 10 mm increasing the total thickness to 136 mm.

Fig. 3 shows the embrittlement trend curve determined using the surveillance weld. The surveillance weld is also based on Phoenix-Union S3NiMo and manufactured using the same procedure as the RPV welds. Table 1 gives the chemical composition of the surveillance weld and the RPV welds. The chemical content of the RPV and the surveillance welds was measured using optical emission spectroscopy (OES) [17]. The median ETC of the surveillance weld follows Eq. (1).

$$\Delta TC_{v\,41J} = 57\left(\frac{\Phi}{10^{19}}\right)^{0.287} \quad (E > 1MeV) \tag{1}$$

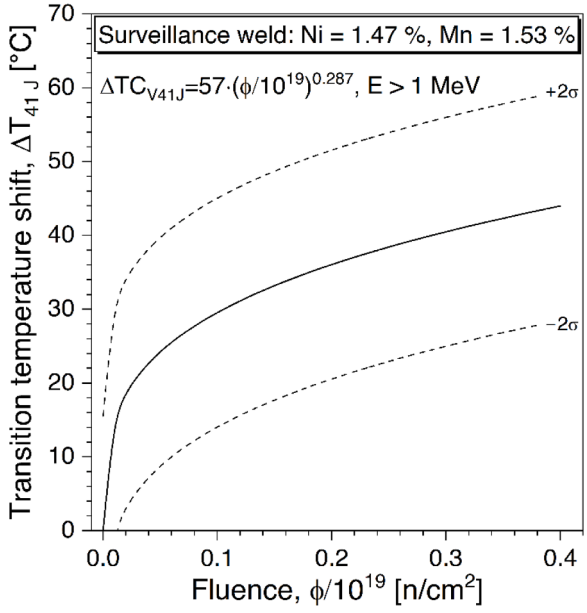

Fig. 3. Shift in impact toughness, TC_{V41J}, due to neutron irradiation. The curve is based on surveillance weld data for Barsebäck 2.

where ΔTC_{V41J} is the impact toughness-based transition temperature determined at 41 J and Φ (n/cm^2) is the fluence.

The surveillance specimens were cut at different locations in the through thickness direction of the manufactured surveillance weld. The specimens were cut in T-S orientation—the crack grows in the thickness direction of the weld and the length of the specimen is transversal to the weld. The surveillance material was tested according to the standards specified in Table 2. The fluence was determined based on a two-dimensional transportation code, DORT.

The microstructure of the weld is characteristic for a multi-layer weld (Fig. 4). Majority of the weld consists of as-welded regions with a dendritic microstructure and between these regions there are the re-heated and twice re-heated regions with equiaxed microstructure. The dendritic microstructure contains mainly acicular ferrite with inter-dendritic grain boundary ferrite, and the equiaxed microstructure contains mainly polygonal ferrite with minor fraction of acicular ferrite. The average axial beltline weld hardness (≈188 HV10) is smaller compared to the RPVH (≈210 HV10) and the circumferential beltline weld (≈214 HV10) [18,19].

2.2. Specimen setup

The orientation of a specimen is determined by the LTS (Longitudinal, Transverse, and short transverse) coordinate system, where the longitudinal coordinate direction is the welding deposit direction [20]. The impact toughness specimens were extracted in T-S orientation corresponding with the Barsebäck 2 surveillance program. On the other hand, the orientation of the tensile specimens was transversal, thus corresponding the loading direction with surveillance program. Specimens were machined using EDM and tested as manufactured. For the circumferential base line weld, the notch of the impact toughness specimens was 8.6 mm from the fusion line. For the axial belt line weld, the distance was 10 mm from the fusion line. For the RPVH weld, the notch was placed at the center of the weld.

2.2.1. Tensile testing

The objective of the tensile testing was to determine the change of strength in trepans to the available data from the surveillance program. The tensile testing procedure was conducted using flat specimens with a rectangular cross-section manufactured and tested in accordance with ISO-6892-1 [21] and 6892-2 [22]. Fig. 5 shows the dimensions of the manufactured specimens. While the specimen size is smaller than defined in the standard, the gauge length and cross-sectional area are proportional to the standards. Prior to the experiment the specimens were measured and validated to be within tolerances with optical dimensional measurement system (OGP CNC Flash 200 MS).

An environmental chamber with nitrogen gas cooling was installed to the test frame. Specimens were tested at temperatures between -120°C and +300°C. The chamber was allowed to settle for at least 30 minutes after the target temperature was initially reached.

The experiments were conducted on a tensile testing machine (Zwick Z250) fitted with a laser extensometer and a 10 kilonewton force transducer (Zwick Xforce K) mounted on the moving crosshead above the specimen. All tests were performed in position control, with a constant speed of 0.12 mm/min throughout the test. This corresponds with the suggested testing rate (method A2, ISO 6892-1) 0.025 % per s of the original parallel length of the specimen. The yield strength is defined as the upper yield strength if it could be identified, or otherwise 0.2 % offset yield strength. Tensile strength corresponds with the maximum force recorded.

2.2.2. Impact toughness testing

The objective of the impact toughness testing was to establish a ductile-to-brittle transition curve, to compare the RPV weld results to the results from the surveillance program. Furthermore, lower transition

Table 1
Chemical composition (wt.%) of Barsebäck 2 RPV, surveillance weld, the RPV head, axial and circumferential beltline weld (BLW) at ¼ thickness.

Material	C	Si	Mn	P	S	Cr	Mo	Ni	Cu	Co	Al
Surveillance	0.084	0.22	1.53	0.011	0.004	0.13	0.44	1.47	0.06	0.008	0.005
RPVH	0.058	0.15	1.40	0.008	0.007	0.04	0.41	1.48	0.06	0.02	0.023
Axial BLW	0.054	0.16	1.43	0.010	0.005	0.03	0.44	1.66	0.07	0.02	0.022
Circ. BLW	0.064	0.16	1.43	0.008	0.005	0.03	0.44	1.66	0.09	0.02	0.078

Table 2
Fluence of the surveillance capsules and applied testing standard. The NPP was operated for 22.7 efpy. In the core region, the temperature is ~275°C.

Applied testing standard		Fluence [n/cm^2] (E > 1 MeV)	Irradiation period
Impact	Tensile		
EN ISO 148-1 and EN ISO 14556	EN ISO 6892-1 method B and EN ISO 6892-2 method B	$5.87{\cdot}10^{19}$	1977-2005
EN ISO 148-1 and EN ISO 14556	EN ISO 6892-1 method B and EN ISO 6892-2 method B	$0.102{\cdot}10^{19}$	1977-2005
EN ISO 148-1 and EN ISO 14556	EN ISO 6892-1 method B and EN ISO 6892-2 method B	$0.102{\cdot}10^{19}$	1977-2005
ASTM E23	ASTM E21	$0.378{\cdot}10^{19}$	1977-2005
ASTM E23	ASTM E21	$0.0575{\cdot}10^{19}$	1977-1990
ASTM E23	ASTM E21	0	

region was emphasized in the testing to establish a crack arrest transition curve from the instrumented impact data. Test temperatures were chosen based on the results for the unirradiated reference data. The Charpy V-notched impact toughness specimens were manufactured as instructed according to ISO 148-1 [16]. Fig. 6 shows the dimensions.

Testing was done in accordance with EN ISO 148 [16,23] and ISO 14556 [24] standards. Impact toughness testing was performed using an instrumented impact machine (Zwick RKP450) with automatic temperature control and feeding system. The employed test setup has a maximum impact capacity of 300 J. The gas-filled temperature control chamber is cooled by circulating liquid nitrogen. Testing was conducted at a temperature range from -180°C to 300°C. Temperature monitoring during conditioning was conducted at both the chamber level and specimen surface. Once the target temperature was reached, the specimen was rapidly moved to the anvil and tested. The instrumentation yields a force-displacement curve from where the unstable crack initiation (F_{iu}), crack arrest (F_a), and the maximum forces (F_m) are determined.

3. Results

3.1. Tensile strength

Fig. 7 illustrates two models for estimating yield strength as a function of temperature: the Zerilli-Armstrong model [25] as implemented by Kirk and the model given in ASTM standard E1921 [26,27]. Both models depend on the yield strength at room temperature. The room temperature yield strength is extrapolated from the mean of the room temperature test results. The Zerilli-Armstrong model results in a less conservative estimate of the temperature behavior at high temperatures. The axial beltline weld is softer compared to the other locations. The base line results represent the reference non-irradiated condition of the surveillance weld.

In contrast, the tensile strength does not continuously decrease with increasing temperature, see Fig. 8. The tensile strength decreases between -100°C and 120°C, but after that there is an increase in strength. The tensile strength of the axial beltline weld is smaller compared to the other locations, similarly to the yield strength. The average standard deviation for yield and tensile strength is 3 MPa.

3.2. Impact toughness

Fig. 9 shows the temperature dependence of the USE. The USE behavior is determined based on the specimens with 100 % ductile tearing. The USE increases between 0°C to 100°C. One outlier is observed at 280°C. The quality of the test is acceptable, the pendulum impact energy and the energy based on the instrumentation are close to each other and the hammer hits the targeted location. Additional tests would be required to understand the behavior at higher temperatures. At temperatures between 0°C to 75°C, the USE for the RPVH weld appears to be lower compared to the other welds, but the difference in mean is insignificant. The average USE for other welds between 0°C and 25°C is 173 J. The standard error of the mean is 14 J, also encompassing the mean for the RPVH.

Fig. 10 shows the impact toughness transition curves, in addition to the un-irradiated reference results from the surveillance program (noted as baseline weld). In the transition region, the axial beltline weld has higher toughness compared to the other welds. Fitting of the transition

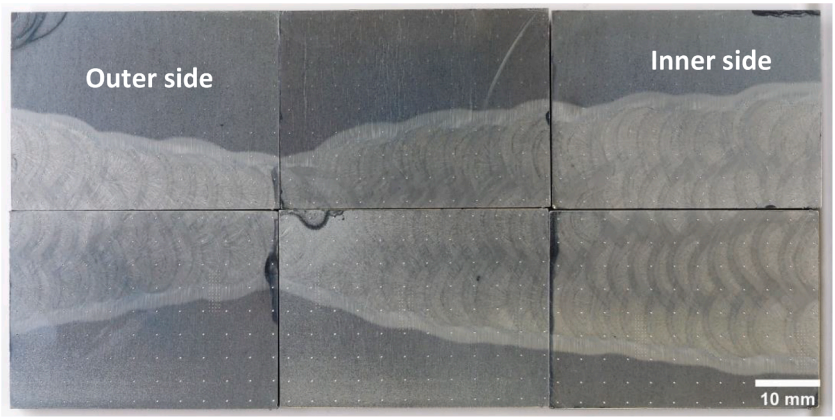

Fig. 4. Through-thickness cut of the Barsebäck RPV multilayer weld.

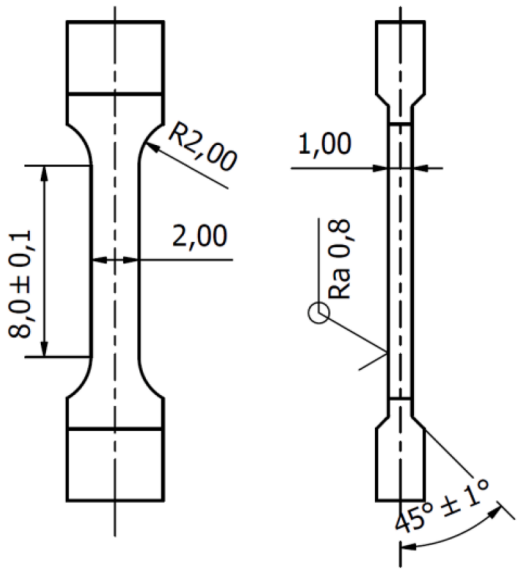

Fig. 5. Tensile specimens. Distance is in millimeters.

curve with respect to the test temperature was done following the methodology described in [28]. The lower shelf energy was fixed at 2 J, and the upper shelf was set at the mean of USE values close to room temperature where fracture appearance was optically determined to be completely ductile. Based on the fitted curves, Table 3 shows the estimated impact toughness transition temperatures at 41 J and 28 J.

3.3. Crack arrest toughness estimation

Materials crack arrest toughness can be estimated from the crack arrest force F_a obtained from an instrumented Charpy V-notch test [28]. The crack arrest forms a transition curve similar to the fracture toughness. The temperature at a crack arrest force of 4 kN (T_{Fa4kN}) correlates well to the crack arrest reference temperature T_{Kla} in steels. The crack arrest force of 4 kN is approximate to a crack jump halfway through the component and is assumed to be large enough to rule out pop-ins from local brittle zones, while small enough to not have the material properties affected by surface effects.

Fig. 11 shows the crack arrest data for the welds. An exponential equation was fitted using the least-squares fitting method:

$$F_a = 4 \cdot \exp\left(\frac{T - T_{Fa4kN}}{A}\right) \quad (2)$$

where A describes the shape of the curve and T is temperature. Specimens with significant crack growth were excluded by applying F_{iu}/F_m (initiation force/maximum force) > 0.7 criterion, otherwise the measured crack arrest force can be lower than the true crack arrest force [30].

For F_a values above 3 kN there are no significant differences between the welds. Closer to the lower shelf the axial beltline weld appears to have marginally higher arrest force, though in that region, the values are not directly comparable since there are less of results for the RPVH and circumferential beltline welds.

The reference crack arrest toughness temperature is estimated using

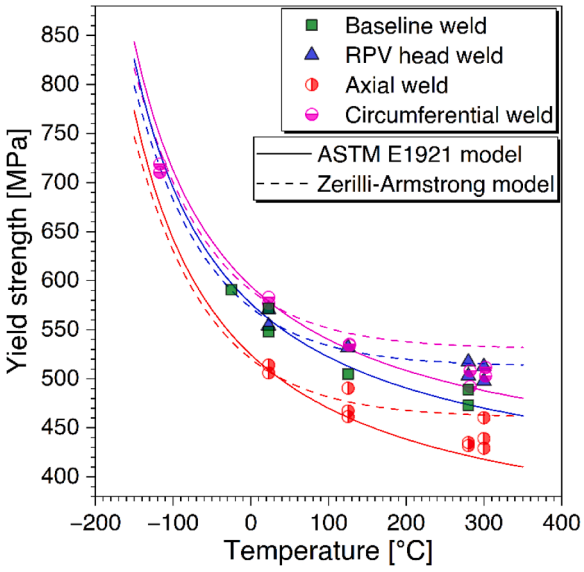

Fig. 7. Yield strength-temperature dependence for baseline, RPVH, and beltline welds.

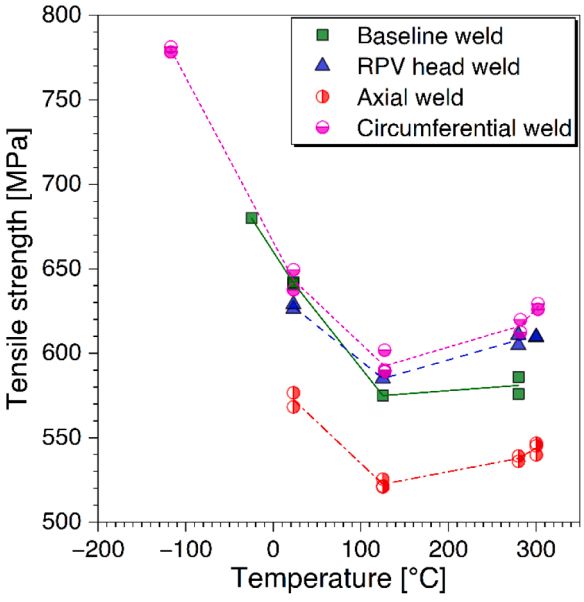

Fig. 8. Temperature dependence of the tensile strength.

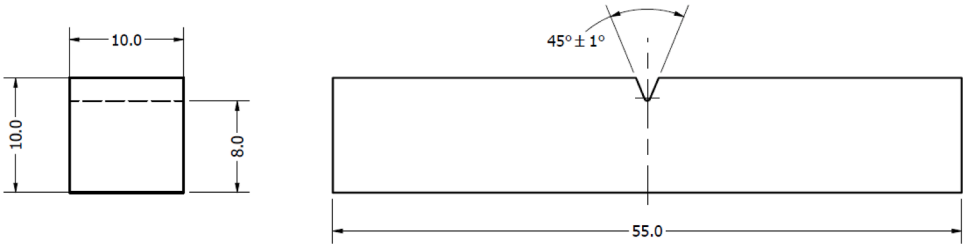

Fig. 6. Illustration of the impact toughness specimens. The dimensions are in mm.

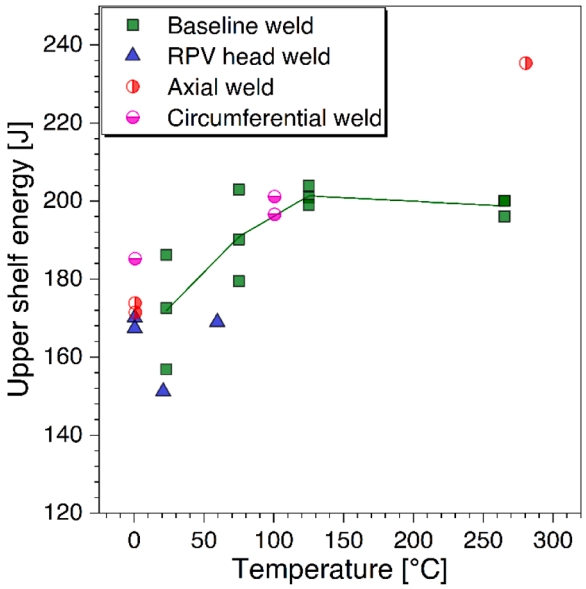

Fig. 9. USE behavior, specimens with 100 % of ductile tearing.

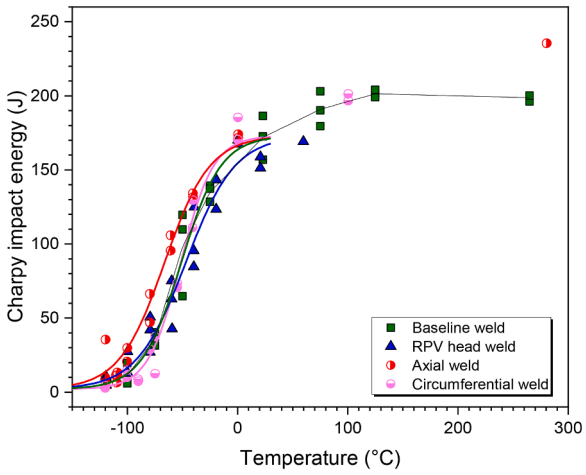

Fig. 10. Impact test energies and transition curves for RPVH and beltline welds.

Table 3
Impact toughness transition temperatures for RPVH, beltline and baseline welds. The standard deviation is determined for transition region, data points between 0.1USE-0.85USE.

	Circumferential beltline	Axial beltline	RPVH	Baseline
$T_{50\%\ US}$ [°C]	-49	-63	-53	-47
T_{41J} [°C]	-70	-95	-75	-75
T_{28J} [°C]	-77	-106	-85	-85
σ [°C]	2.8	10.1	9.7	7.6
95 CI%*	± 3.4	± 7.6	± 7.4	± 5.9

*For transition temperature estimates

Eq. (3),

$$TK_{la} = T_{Fa4kN} + 11.4\ ^{\circ}C \quad (3)$$

with $\sigma TK_{la} = 12.0\ ^{\circ}C$ [28]. In Table 4, the T_{Fa4kN} crack arrest force for each weld is presented along with its corresponding T_{Kla} temperature.

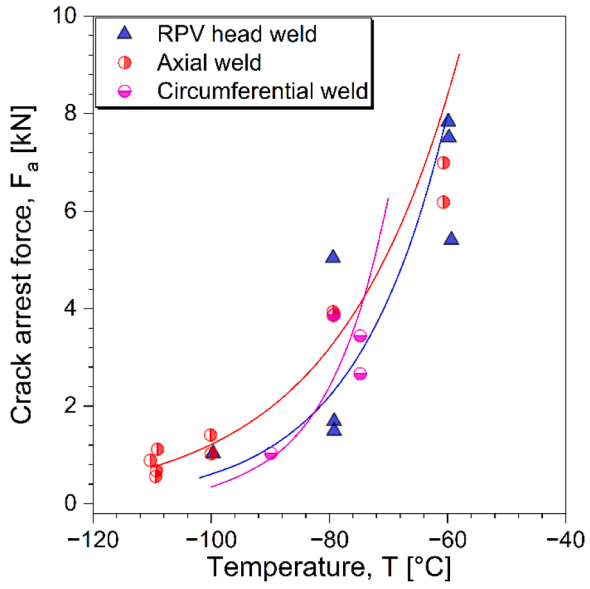

Fig. 11. Crack arrest force-temperature curves.

Table 4
Crack arrest force corresponding to 4 kN and the estimated crack arrest toughness.

[°C]	Circumferential	Axial	RPVH
T_{Fa4kN}	-71 ± 2	-74 ± 3	-70 ± 9
T_{Kla}	-60 ± 14	-63 ± 15	-59 ± 21

4. Discussion

4.1. Factors affecting the variations in mechanical properties

The axial beltline weld is softer and the impact toughness is higher in the transition region compared to the other locations. Based on the chemical composition, the axial and circumferential beltline welds are similar, see Table 1. The circumferential beltline weld has possibly marginally higher carbon content, 0.064 % compared to 0.054 % in the axial beltline weld. All welds were manufactured according to the same guidance and hence similar welding parameters. The nominal post-weld heat-treatment temperature and time are the same for the circumferential and axial beltline weld.

However, the welding guidance allows variations of ±15°C in the post-weld heat treatment. Variations in the PWHT temperature and time can explain the differences in mechanical properties. The combined effects of time and temperature during PWHT is investigated using Hollomon-Jaffe relationship:

$$TP = \frac{T}{1000} \cdot (C + \log(t)) \quad (4)$$

where TP is the Hollomon-Jaffe parameter, T is temperature in kelvin, t is soaking time in hours, and C is a constant which is typically 20 for steels with a carbon content of 0.06 %. The TP parameter describing the effects of the heat treatment on the material correlates with changes in mechanical properties. [29] In [29], a cast nodular iron alloy was investigated. They observed that for TP-values between 16 and 20 for different initial hardness levels, the Vickers hardness (HV) decreases linearly with increasing TP according to Eq. (5),

$$\Delta HV = -38.5 \cdot \Delta TP \quad (5)$$

In [30], they investigated the PWHT soaking time for a multi-pass shielded, metal arc welded Cr-Mo high strength low alloy steel, ASTM

A 213. The PWHT soaking temperature was 725°C and the time varied. The results show that for soaking times between 2 h – 10 h the strength reduces and impact toughness increases. The hardness reduction follows Eq. (5).

Thus, a possible reason for the difference in the impact toughness and in hardness between the axial and circumferential beltline weld is the heat treatment. It is possible that the axial beltline weld actually had a higher temperature during PWHT than the circumferential weld (case 1). Another possibility is that, as the investigated axial weld is relatively close to the circumferential beltline weld, the axial weld was subjected to a PWHT twice the time of the circumferential weld (case 2). The axial weld was manufactured first and after that welded together with the other pieces of the RPV.

Table 5 shows the extremities of the heat treatments of the axial and circumferential weld. The TP parameter is estimated based on possible upper/lower limits for temperature and time given in Table 5. Assuming that PHWT temperature is actually 605°C (= 620°C -15°C) for the circumferential and 635°C for the axial beltline weld, the predicted and measured hardness differences between the welds are then close to each other, see Table 5. If the PWHT time of the axial beltline weld would be two times longer, the hardness difference would increase with an additional 11 HV. The prediction is based on the assumption that Eq. (5) derived from data in [29] can be applied to the investigated material. At least, the TP-HV values from this study overlap with the results from [29] between TP values of 16 and 20.

Generally, the permitted variations in the heat treatment parameters give a likely explanation to the differences in the material properties between the circumferential and axial beltline weld. Future work will focus on microstructural characterization of the results to understand even better the differences. In addition, the effect of residual stresses of the axial and circumferential welds could be a factor to be accounted for.

4.2. The embrittlement behavior

Fig. 12 shows the shifts in T_{41J} for the beltline welds at ¼ thickness, i.e., at the extraction location. The Fig. contains also a through-thickness prediction of the shift in T_{41J} based on the surveillance data, Eqs. (1), and (6) for estimation of fluence attenuation [31].

$$\phi = \phi_{surface} \cdot e^{-0.24 \cdot (x/25.4)} \quad (6)$$

where $\phi_{surface}$ is the fluence at the surface and x is the distance from the inner surface in mm. Table 6 gives the measured fluence at the surface of the belt line weld trepans before removal of the cladding.

For the circumferential beltline weld, the experimental data does not differ significantly from the prediction. At ¼ thickness for the axial beltline weld, the prediction indicates a ≈5°C shift in T_{41J}. However, the axial beltline weld is tougher compared to the prediction based on the surveillance data. The surveillance data describes the aging behavior of the circumferential beltline weld and gives a conservative prediction for the axial beltline weld. This result underlines that knowledge of the manufacturing parameters is important for assessing the mechanical properties.

The high-Ni/Mn materials can be sensitive to thermal aging and the effect can be significant [9,32]. At low fluence levels, the effect of thermal embrittlement can be larger than the effect of irradiation embrittlement. The existing predictions for thermal embrittlement of high-Ni/Mn welds are based on VVER-1000 materials. In [32], the prediction for transition temperature shifts due to thermal aging (ΔT_T) is dependent on Ni, T_{K0} (= the impact toughness-based transition temperature defined as described in [33]) and time, t:

$$\Delta T_T = 1.3 Ni^4 \exp(-0.02 T_{K0}) \left(1 - exp\left(-1.1 \cdot 10^{-5} \cdot t\right)\right)^{0.6}, (\pm 18°C) \quad (7)$$

Eq. (7) is based on VVER-1000 welds with 1.1 % < Ni < 1.89 %, 0.7 % < Mn < 1.00 %, 0.006 % < P < 0.009 %, the material was subjected to a temperature of 310°C–320°C for 200 000 h [32].

For the investigated material, Fig. 13 shows that the effect of thermal aging on T_{41J} shift is insignificant. The assessment is based on a comparison between the unirradiated reference data from the surveillance program and the RPVH results. The prediction based on Eq. (7) results in a conservative estimate (a higher shift) of the embrittlement. One significant difference compared to Eq. (7) is the aging temperature, which is 288°C for the investigated material. The aging mechanisms related to thermal aging are not necessarily activated or are slower at lower temperatures [34], thus Eq. (7) based on aging at 310°C–320°C is not directly applicable for the investigated material.

The existing ETCs are less suitable for high-Ni/Mn welds. They do not tend to account for the synergetic effect of Ni and Mn which can have a significant impact on the trend curve. The ETC developed based on the French data, the FFI correlation [3,35], is valid for Ni < 1.4 % and Mn

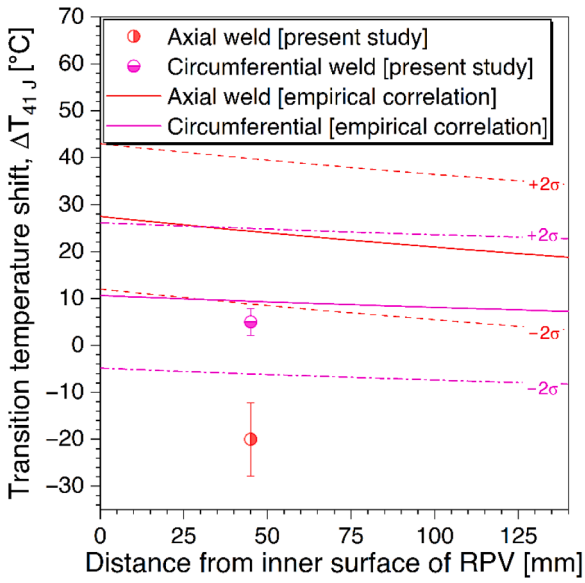

Fig. 12. Shift in T_{41J} due to irradiation embrittlement for the circumferential and the axial beltline welds at ¼ thickness.

Table 6
The fluence of the beltline trepans.

Weld location	Fluence at surface [n/cm^2] (E > 1 MeV)	Fluence at ¼ T [n/cm^2]
Axial	$7.9 \cdot 10^{17}$	$3.8 \cdot 10^{17}$
Circumferential	$2.9 \cdot 10^{16}$	$1.4 \cdot 10^{16}$

Table 5
The effect of PWHT time and temperature on hardness. Beltline weld (BLW).

Weld	PWHT t [h]	PWHT T [°C]	TP	Prediction ΔHV compared to circumferential beltline weld	Measured ΔHV compared to circumferential beltline weld
Circumferential BLW	5.5	605	18.2	0	0
Axial BLW	5.5	635	18.8	-24	-26
Axial BLW	11	635	19.1	-35	-26

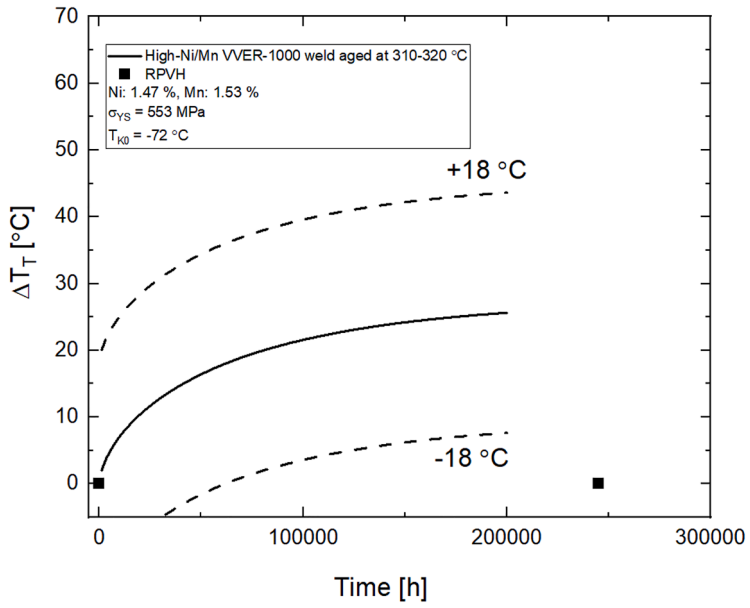

Fig. 13. The effect of thermal aging at 288°C for 240 000 h on the T_{41J} shift.

between 1.2 %–1.9 %. The trend curve is dependent on Ni but not on Mn. The FFI ETC is based on surveillance data (900 MWe reactors) and it is complemented with test reactor data. The E900 ETC is valid for Ni contents < 1.7 % and Mn contents between 0.55 %–2 %. The prediction is dependent on Ni and Mn. In Table 7, the validity ranges for the ETC are given in more detail, and a comparison is made to the investigated weld.

Based on VVER-1000 weld metal data, consisting of high-Ni/Mn welds, a synergetic dependence between Ni and Mn has been developed, [37]:

$$\Delta T_K = 1.68 C_{Ni} C_{Mn} F^{0.8}, \ (\sigma = 13.5\ ^\circ C) \tag{8}$$

where F is the fluence ($\cdot 1/10^{22}$ n/m^2). The Fluence is based on neutrons with an energy of E > 0.5 MeV. To convert it to E > 1 MeV, so that a comparison can be made to the Barsebäck 2 surveillance data, Eq. (1), the following dependence is used [8]:

Table 7
Validity ranges for common predictions and comparison to the Barsebäck welds. The bold texts in the cells indicate that the Barsebäck parameters are within the limits of the prediction. The predictions are valid up to significantly higher fluences compared to the Barsebäck surveillance data.

	E900-21 [36] Validity range %	FFI [3,35]	VVER-1000 weld	Barsebäck 2 surveillance weld
Ni	***< 1.7***	0.07 – 1.4	***1.2–1.9***	1.47
Cu	***< 0.4***	***0.02 – 0.13***	***0.05–0.08***	0.06
P	***< 0.03***	***0.003 – 0.021***	***< 0.025***	0.011
Mn	***0.55 – 2***	***1.2 – 1.9***	0.5–1.1	1.53
Ni and Mn effect	Separate effect, C_{Ni}+C_{Mn}	Only C_{Ni} accounted for	Combined effect, $C_{Ni}C_{Mn}$	
Dependence dependent on	T_{irr}, fluence (E > 1 MeV), Cu, Ni, P, Mn	Fluence (E > 1 MeV), Cu, Ni, P	Ni, Mn, Fluence (E > 0.5 MeV)	
$T_{irradiation}$	***255 – 300°C***	***Mostly above 288°C***	***290–320°C***	288°C
Reactor type	***BWR and PWR***	PWR	PWR	BWR

$$\frac{F(E > 0.5\ MeV)}{F(E > 1\ MeV)} \propto 1.78 \tag{9}$$

Fig. 14 compares the ETC predictions to the Barsebäck 2 surveillance data. For the FFI and VVER-1000 models within the investigated fluence range, the upper bound of the prediction encompasses the mean of the Barsebäck 2 surveillance curve. The Barsebäck surveillance curve is steeper in the beginning compared to the VVER-1000 and FFI prediction. Both of those predictions are based on data from PWR reactors where the neutron flux can differ from a BWR reactor. The Barsebäck 2 weld metal has higher Ni content than allowed by the FFI prediction and higher Mn content than allowed by the VVER-1000 prediction. The ASTM E900 prediction has better agreement with the Barsebäck data, the chemistry is within the limits, and the E900 prediction is based on both BWR and PWR data. In addition, the E900 prediction accounts better for time dependent effects of the embrittlement behavior.

In [5], the results indicate the presence of the synergetic effect of Ni and Mn on embrittlement after the combined Ni and Mn content exceeds 2.9 %. After the limit is exceeded, the existing ETCs are less applicable. [5] For the investigated weld, the combined effect of Ni and Mn increases above that limit. The applied ETCs underpredict the embrittlement behavior, but the difference to the mean behavior is smaller than the uncertainty, though for the FFI and the VVER predictions the upper part of the uncertainty band just encompasses the Barsebäck surveillance curve. However, due to a relatively good prediction of the embrittlement behavior, especially using the E900 prediction, the possible synergetic effect of Ni and Mn appears to be less significant at lower fluences.

5. Conclusions

High-Ni/high-Mn welds from decommissioned Barsebäck 2 RPV were investigated. The welds were extracted from the RPVH, the circumferential and axial beltline welds, enabling comparison between the RPVH material subjected to a relatively high temperature, and the beltline region subjected to neutron irradiation and high temperature. The mechanical properties were characterized at ¼ thickness, including instrumented Charpy-V testing according to ISO-148-1 and tensile testing according to ISO 6892-1. The results are compared to the surveillance program.

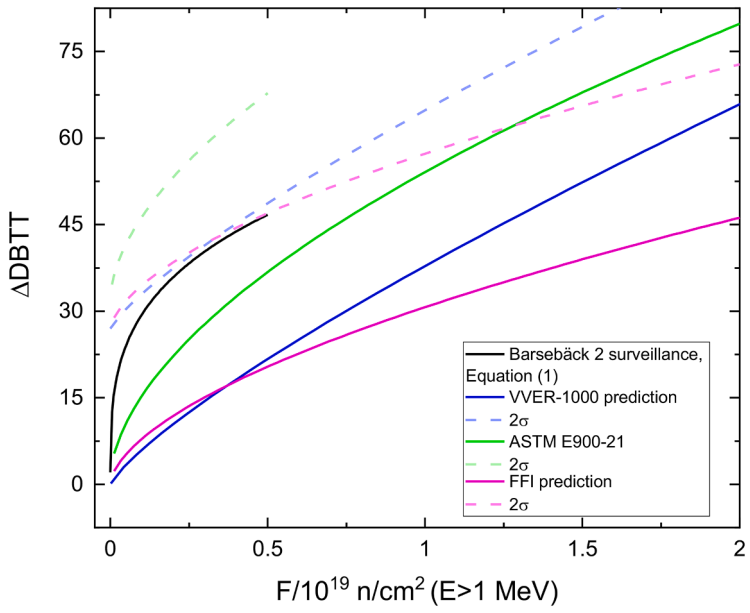

Fig. 14. The mean embrittlement curve for Barsebäck 2 (B2) surveillance weld compared to ETC predictions. Predictions are based on B2 surveillance weld chemistry, see Table 7.

- The embrittlement trend curve based on the impact toughness results from the surveillance program describes the embrittlement behavior of the RPV welds subjected during operation to a temperature close to 270°C, irradiation (maximum fluence being $7.9{\cdot}10^{17}$ n/cm^2) and pressure. The surveillance data describes the aging behavior of the circumferential beltline weld and gives a conservative prediction of the axial beltline weld.
- Compared to the surveillance, RPVH and circumferential beltline welds, the axial beltline weld is softer and impact toughness is higher. The yield strength of the non-irradiated surveillance, RPV head and circumferential welds is close to 565 MPa at room temperature, and T_{41J} is close to -73°C. For the axial beltline weld yield strength is 510 MPa at room temperature and T_{41J} is -95°C. The chemistry of the axial and the circumferential weld is similar.
- The differences in mechanical properties possibly originate from variations in the PWHT temperature and time. A PWHT temperature difference of 30°C, allowed by the welding guidance, can cause a change in hardness equal to the difference observed between the axial and circumferential beltline weld.
- The RPVH weld impact toughness results are comparable to the reference condition even after 23 effective full power years operation at 288°C, and thus no conclusive thermal embrittlement is identified based on impact toughness testing.
- The ASTM E900, FFI and VVER embrittlement trend curve predictions encompass the average embrittlement behavior of the investigated high-Ni/Mn (Ni $>$ 1.5 %, Mn $=$ 1.5 %) weld in the low fluence region ($< 0.5{\cdot}10^{19}$ n/cm^2, E $>$ 1 MeV). In this perspective, the synergetic effect of Ni and Mn appears to be less significant at lower fluences. ASTM E900 prediction describes better the investigated weld compared to the VVER and FFI predictions.

CRediT authorship contribution statement

Sebastian Lindqvist: Conceptualization, Formal analysis, Writing – original draft. **Alex Norrgård:** Investigation, Writing – original draft. **Pentti Arffman:** Formal analysis, Software, Writing – review & editing. **Noora Hytönen:** Investigation, Writing – review & editing. **Jari Lydman:** Investigation. **Pål Efsing:** Resources, Writing – review & editing. **Siddharth Suman:** Writing – review & editing. **Pekka Nevasmaa:** Supervision.

Declaration of Competing Interest

The authors declare that they have no known competing financial interests or personal relationships that could have appeared to influence the work reported in this paper.

Data availability

Data will be made available on request.

Acknowledgements

BRUTE (Barsebäck RPV material used for true evaluation of Embrittlement) is an Excellence project in the SAFIR2022 program, which is funded by VYR (Nuclear Waste Management Fund in Finland), VTT Technical Research Centre of Finland and NKS (Nordisk Kärnsäkerhet). The amount of in-kind contribution from the BREDA (Barsebäck Research & Development Arena) project is substantial as BREDA has planned, funded and executed the cutting of the trepans used in BRUTE. Thank you also to Jenny Roudén, Vattenfall, for technical discussions. The funding, access to plant relevant material and support from the supporting organizations is highly appreciated.

References

[1] IAEA, Integrity of reactor pressure vessels in nuclear power plants: assessment of irradiation embrittlement effects in reactor pressure vessel steels, 2009.
[2] W.L. Server, Irradiation embrittlement of reactor pressure vessels (RPVs) in nuclear power plants, 2015. https://doi.org/10.1533/9780857096470.1.3.
[3] W.L. Server, M. Brumovský, International review of nuclear reactor pressure vessel surveillance programs. STP1603, 2018. https://doi.org/10.1520/stp1603-eb.
[4] ASTM E185-16, Standard practice for design of surveillance programs for light-water moderated nuclear power reactor vessels. ASTM E185-16, ASTM International, 2016, https://doi.org/10.1520/E0185-16.Copyright.
[5] M. Kolluri, P. ten Pierick, T. Bakker, B.T. Straathof, A.J. Magielsen, Z. Szaraz, E. D'Agata, C. Ohms, O. Martin, Influence of Ni-Mn contents on the embrittlement of PWR RPV model steels irradiated to high fluences relevant for LTO beyond 60 years, J. Nucl. Mater. 553 (2021), 153036, https://doi.org/10.1016/j.jnucmat.2021.153036.
[6] IAEA-TECDOC-1441, Effects of nickel on irradiation embrittlement of light water reactor pressure vessel steels, IAEA, Vienna, 2005.
[7] A.M. Kryukov, D.Y. Erak, L. Debarberis, F. Sevini, B. Acosta, Extended analysis of VVER-1000 surveillance data, Int. J. Press. Vessels Pip. 79 (2002) 661–664, https://doi.org/10.1016/S0308-0161(02)00069-8.

[8] L. Davies, A comparison of Western and Eastern nuclear reactor pressure vessel steels, Int. J. Press. Vessels Pip. 76 (1999) 163–208, https://doi.org/10.1016/S0308-0161(97)00075-6.
[9] M. Boåsen, K. Lindgren, M. Öberg, M. Thuvander, J. Faleskog, P. Efsing, Analysis of thermal embrittlement of a low alloy steel weldment using fracture toughness and microstructural investigations, Eng. Fract. Mech. (2022), 108248, https://doi.org/10.1016/j.engfracmech.2022.108248.
[10] M. Valo, A. Amaev, R. Ahlstrand, D. Chistiakov, E. Krasikov, A. Kryukov, A. Morosov, V. Nikolaev, P. Platonov, R. Rintamaa, V. Rybin, Y. Shtrombakh, K. Wallin, Characterization of the decommissioned novovoronesh-1 pressure vessel wall materials by through-wall trepans, in: Effects of Radiation on Materials: 19th International Symposium, ASTM International, 100 Barr Harbor Drive, PO Box C700, West Conshohocken, PA 19428-2959, 2000: pp. 98-98–20. https://doi.org/10.1520/STP12385S.
[11] D.E. McCabe, R. Nanstad, S. Iskander, R.L. Swain, Unirradiated material properties of Midland weld WF-70, (1994).
[12] M.A. Sokolov, R.K. Nanstad, Fracture toughness characterization of midland beltline weld after high dose of irradiation, in: volume 7: operations, applications, and components, ASMEDC, 2006: pp. 85–89. https://doi.org/10.1115/PVP2006-ICPVT-11-93321.
[13] U. Rindelhardt, H.-W. Viehrig, J. Konheiser, J. Schuhknecht, K. Noack, B. Gleisberg, RPV material investigations of the former VVER-440 Greifswald NPP, Nucl. Eng. Des. 239 (2009) 1581–1590, https://doi.org/10.1016/j.nucengdes.2008.07.018.
[14] H.-W. Viehrig, E. Altstadt, M. Houska, M. Valo, Fracture mechanics characterisation of the beltline welding seam of the decommissioned WWER-440 reactor pressure vessel of nuclear power plant Greifswald Unit 4, Int. J. Press. Vessels Pip. 89 (2012) 129–136, https://doi.org/10.1016/j.ijpvp.2011.10.016.
[15] H.-W. Viehrig, J. Schuhknecht, Fracture mechanics characterisation of the WWER-440 reactor pressure vessel beltline welding seam, Int. J. Press. Vessels Pip. 86 (2009) 239–245, https://doi.org/10.1016/j.ijpvp.2008.11.001.
[16] SFS-EN ISO 148-1, Metallic materials. Charpy pendulum impact test. Part 1: test method, (2016).
[17] N. Hytönen, Effect of microstructure on brittle fracture initiation in a reactor pressure vessel weld metal, (2019).
[18] Z. Que, M. Lindroos, J. Lydman, N. Hytönen, S. Lindqvist, P. Efsing, P. Nevasmaa, P. Arffman, Brittle fracture initiation in decommissioned boiling water reactor pressure vessel head weld, J. Nucl. Mater. 569 (2022), 153925, https://doi.org/10.1016/j.jnucmat.2022.153925.
[19] N. Hytönen, Z. Que, P. Arffman, J. Lydman, P. Nevasmaa, U. Ehrnstén, P. Efsing, Effect of weld microstructure on brittle fracture initiation in the thermally-aged boiling water reactor pressure vessel head weld metal, Int. J. Minerals Metallurg. Mater. 28 (2021) 867–876, https://doi.org/10.1007/s12613-020-2226-6.
[20] ASTM E399-20, Standard Test Method for Linear-Elastic Plane-Strain Fracture Toughness of Metallic Materials, ASTM International, 2020.
[21] SFS-EN ISO 6892-1, Metallic materials. Tensile testing. Part 1: method of test at room temperature, (2019).
[22] ISO 6892-2, Metallic materials. Tensile testing. Part 2: method of test at elevated temperature, (2018).
[23] SFS-EN ISO 148-2, Metallic materials. Charpy pendulum impact test. Part 2: verification of testing machines, (2016).
[24] SFS-EN ISO 14556, Metallic materials. Charpy V-notch pendulum impact test. Instrumented test method, (2015).
[25] F.J. Zerilli, R.W. Armstrong, Dislocation-mechanics-based constitutive relations for material dynamic calculations, J Appl Phys 61 (1987) 1816–1825.
[26] M.T. Kirk, The technical basis for application of the master curve to the assessment of nuclear reactor pressure vessel integrity, United States Nuclear Regulatory Commission, 2002.
[27] ASTM E1921-21, Standard test method for determination of reference temperature, to, for ferritic steels in the transition range, (2021). https://doi.org/10.1520/E1921-21.
[28] K. Wallin, Fracture Toughness of Engineering Materials, EMAS Publishing, Warrington, UK, 2011, 1st ed.
[29] F.S. Vicente, J.C. Carrasco, R.F. Antoni, J. Carlos, F. Taberner, M.P. Guillamón, Hardness prediction in quenched and tempered nodular cast iron using the Hollomon-Jaffe parameter, Metals (Basel) 11 (2021).
[30] S.R. Ahmed, L.A. Agarwal, B.S.S. Daniel, Effect of different post weld heat treatments on the mechanical properties of Cr-Mo Boiler steel welded with SMAW Process. 4th International conference on Materials Processing, Mater. Today Proc. (2015) 1059–1066, https://doi.org/10.1016/j.matpr.2015.07.002.
[31] Regulatory guide 1.99 - radiation embrittlement of reactor vessel materials, Revision 2 (1988).
[32] B.A. Gurovich, A.A. Chernobaeva, D.Y. Erak, E.A. Kuleshova, D.A. Zhurko, V. B. Papina, M.A. Skundin, D.A. Maltsev, Chemical composition effect on VVER-1000 RPV weld metal thermal aging, J. Nucl. Mater. 465 (2015) 540–549, https://doi.org/10.1016/j.jnucmat.2015.06.010.
[33] K. Wallin, Comparison of the scientific basis of Russian and European approaches for evaluating irradiation effects in reactor pressure vessels, (1994).
[34] G. Gage, S.G. Druce, E.W. Popkiss, Thermal ageing embrittlement of the heat-affected zone in a PWR RPV steel weldment. Proceedings of the topical meeting on nuclear power plant life extension, (1988).
[35] P. Todeschini, Y. Lefebvre, H. Churier-Bossennec, N. Rupa, G. Chas, C. Benhamou, Revision of the irradiatio embrittlement correlation used for the EDF RPV fleet, in: Fontevraud 7 (2010).
[36] ASTM-E900-21, Standard guide for predicting radiation-induced transition temperature shift in reactor vessel materials, 2021.
[37] D. Erak, B. Gurovich, E. Kuleshova, Y. Shtrombakh, D. Zhurko, V. Papina, Radiation embrittlement of VVER-1000 reactor pressure vessel materials, in: SMiRT-22, Conference on Structural Mechanics in Reactor Technology, 2013.